High-resolution X-Ray spectral diagnostics of Active Galactic Nuclei

Steenbrugge, K.C.

Chapter 6

Modeling broad X-ray emission lines observed in NGC 5548

K.C. Steenbrugge, J.S. Kaastra, D. M. Crenshaw, S. B. Kraemer, N. Arav,
E. Costantini, I. M. George

To be submitted to Astronomy & Astrophysics

Abstract

We discuss the detection in the X-ray band of broad emission lines, similar to the broad emission lines detected in the optical and the UV bands, in the Seyfert 1 galaxy NGC 5548. Simultaneous HST STIS observations allow us to model the line strengths measured in the X-ray and the UV band. We determined how the line luminosity is dependent on the input parameters and assumed spectral energy distribution. Unless the density is very high or the covering factor rather low, differences in density, covering fraction and elemental abundances and column density were negligible in both codes. Also the spectral energy distribution used has a negligible effect on the line luminosity predictions. To restrict the possible parameter space, we assumed that the broad line clouds were at a distance of either 2 light days (shortest reverberation distance) or 20 light days (reverberation distance of the Hβ line). We can model the lines with a cloud with one ionization parameter, which is the same for both distances. However, the total column density and the covering factor are larger for the 2 light-day models. This suggests that the region has a density stratification by a factor of 100, rather than an

ionization stratification. The ten times larger total column density and 2.5 times larger covering factor are consistent with a our line of sight crossing the edge of a cloud.

6.1 Introduction

In 1943 Seyfert detected broadened emission lines in the optical spectra in the centers of nearby galaxies. These AGN are now called Seyfert galaxies, and have line widths of several thousands to tens of thousands of km s^{-1}. These emission lines are now used to classify active galaxies as Seyfert galaxies; and they have been well studied in the optical and UV range of the spectrum. Variability studies of these broad emission lines (BEL's) spanning several years found that the lines are variable. The Broad Line Region (BLR) is spatially unresolved using ground based telescopes. However, reverberation mapping (Blandford & McKee 1982) allows for a determination of the size of the BLR, which span a range from a few light-days to light-months.

The broadening of these emission lines is generally thought to be due to the Doppler effect as originally suggested by Seyfert (1943). In the scenario of McKee & Tarter (1975) the broad emission lines are the result of a large number ($\gg 10^6$) of clouds in Keplerian rotation around the central super-massive black hole. The main problem with this scenario is that in high signal-to-noise cross-correlation studies of the broad lines in the UV band, no correlation signal in emission line profile was detected. Further, any line profile variations are not correlated to continuum variability and the velocity fields are not dominated by radial motion, as there is no correlation between the time lag observed and the radial velocity (Peterson 1994). In the case of NGC 4151, the lack of correlation signal in the line profiles in the cross-correlation of high signal to noise spectra, puts a lower limit on the number of clouds of 3×10^7 (Arav et al. 1998). This number exceeds, by an order of magnitude, the number of clouds expected from photoionization models (Arav et al. 1998). If the clouds are small, as required from the large number of clouds and the small measured covering fraction, the radiation pressure should dominate over the gravitational force, as radiation pressure is inversely related to the radius of the cloud. This means that the clouds should form an outflow, which is not observed (Peterson 1994). However, there is not yet a good alternative to the clouds model.

Until the advent of XMM-*Newton* and *Chandra* such broad emission lines were not detected in the X-rays. XMM-*Newton* detected relativistically broadened emission lines in several AGN (Lyα lines from hydrogenic CNO, Branduardi-Raymont et al. 2001; Fe Kα, Wilms et al. 2001) similar to the first Fe K lines discovered by ASCA (Tanaka et al 1995). However, these lines are formed very close to the black hole, in a different region from the BLR, and will not be discussed in this paper. The first de-

tection of a broad emission line in the X-ray band was the C VI Lyα line found in a 90 ks exposure of NGC 5548 with the Low Energy Transmission Grating spectrometer (LETGS) onboard of *Chandra* (Kaastra et al. 2002a). A later XMM-*Newton* observation of the same source in a brighter state did not show such a broad emission line, probably because the higher flux level further decreased the contrast level. A C VI Lyα broad emission line was detected in the spectrum of NGC 4051, which is dominated by relativistically broadened emission lines from O VIII (Ogle et al. 2004). Also in Mrk 279 several broad X-ray emission lines have been detected (Costantini et al. 2005).

For NGC 5548 photoionization and variability studies of the optical broad emission lines have shown that a single zone emitter is insufficient for proper modeling the BLR (Peterson 1994). A stratified zone with either a constant ionization parameter U or constant density n is adequate to fit the lowly ionized versus highly ionized UV broad emission line ratios. From an analysis of the time variability, a constant ionization model better describes the broad line emitting clouds (Goad & Koratkar 1998). In this scenario the density is proportional to r^{-2}, with r the distance from the ionizing source. From reverberation mapping the BLR size of NGC 5548 is found to range between 2 ld, the timescale on which variability is detected in He II (Peterson & Wandel 1999) and 20 ld, the timescale of variability in Hβ (Peterson et al. 1994). The covering fraction is about 30 %, higher than the standard 10 % (Goad & Koratkar 1998). In this paper we investigate whether the higher ionized X-ray lines can be modeled with one ionization parameter and are formed at the same distance, or whether multiple ionization parameters are necessary.

In this paper we analyze the broad emission lines which are observed in a 540 ks *Chandra* observation of NGC 5548 and a simultaneous HST STIS observation. As a result we can model both the X-ray and UV broad emission lines together. In Sect. 6.2 an overview of the analysis of the continuum spectrum and the warm absorber observed in the X-rays and the UV band is given. In Sect. 6.3 we discuss the detection and fitting of the broad emission lines in both spectral bands. The model predictions obtained from XSTAR 2.1h (Kallman & Krolik 1999) and CLOUDY 95.06 (Ferland 2002) are detailed and compared to the measured line luminosities in Sect. 6.4. In Sect. 6.5 we discuss the results obtained from both codes and list the conclusions.

6.2 The X-ray and UV spectrum of NGC 5548

NGC 5548 was observed for a full week with the *Chandra* High Energy Transmission Grating Spectrometer (HETGS) and the Low Energy Transmission Energy Grating (LETGS) in January 2002. Simultaneous HST STIS observations were obtained,

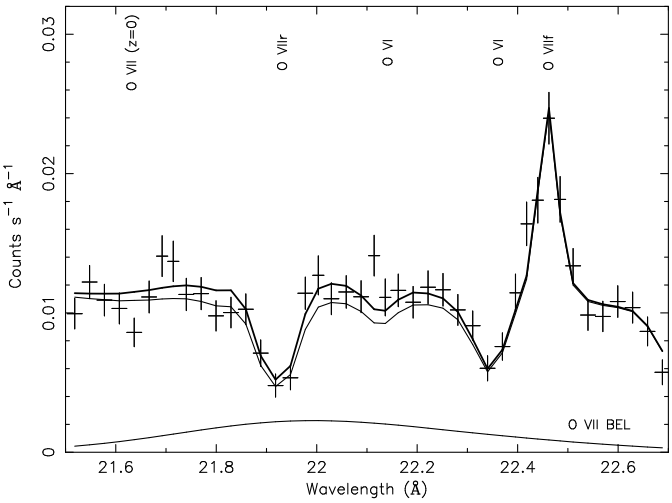

Figure 6.1: Detail of the LETGS spectrum showing the fit with (thick line) and without (thin line) a broad emission line for the O VII resonance line. The profile of the O VII broad emission line is also plotted.

and the analysis of the UV absorber is discussed by Crenshaw et al. (2003). A full analysis of the X-ray spectrum is given by Steenbrugge et al. (2004). We refer to that paper for full details about the analysis, a description of the warm absorber fitting and modeling of the continuum. No spectral variability in the warm absorber was detected and therefore the full dataset was used in order to maximize the signal to noise ratio.

The continuum of NGC 5548 was fit by a power-law and a modified black body component (Kaastra & Barr 1989) corrected for Galactic extinction ($N_{\rm H}$ = 1.65 $\times$ 10^{24} m^{-2}, Nandra et al.1993) and a cosmological redshift of 0.01676 (Crenshaw & Kraemer 1999). An excellent fit to the spectra was obtained using either an absorption model with three outflow velocities (model A of Steenbrugge et al. 2004) or an absorption model with a power-law distribution of the hydrogen column density $N_{\rm H}$ versus the ionization parameter ξ (model D). As found earlier (Steenbrugge et al. 2003) the higher ionization gas in NGC 5548 has a higher total hydrogen column density than the lower ionized gas. The final model includes some narrow emission lines, most notable the O VII forbidden line and the Fe Kα line.

6.3 Broad emission lines

6.3.1 X-ray broad emission lines

The data show a clear broad excess over the spectral fit (thin line Fig. 6.1) at the O VII triplet wavelength (see Fig. 6.1). Broad excesses at other wavelengths are also observed, but they are weaker.

From UV spectra it is clear that these broad lines have complex shapes, and each line can have a different width and line profile (Arav et al. 2002). Due to the lower spectral resolution and signal to noise ratio of the *Chandra* spectra as compared with the optical and UV band spectra, we need to constrain the fit for the broad lines. The broad excesses were fit with Gaussians, leaving the normalization as a free parameter, but freezing the energy to the rest energy of the line and the full width half maximum (FWHM) to 8000 km s^{-1}. This FWHM was taken from Arav et al. (2002) for the broadest component of C IV and Lyα emission line. Kaastra et al. (2002a) measure a FWHM of 10600 km s^{-1} $\pm$ 3300 km s^{-1} for the C VI Lyα line in an earlier LETGS observation of NGC 5548, consistent with the value adopted here. In Table 6.1 we summarize the measured flux, luminosity (L), and Equivalent Width (EW) for the observed lines in the *Chandra* spectra.

The most pronounced of these broad emission lines in the X-rays is the one centered on the O VII triplet. This is in agreement with expectations as oxygen is the most abundant metal and the resonance, intercombination and the forbidden line produce one broad blend. The spectral separation between the triplet components of 0.2–0.3 Å is small compared to the intrinsic FWHM of the lines (0.6 Å). Therefore it is not possible to derive the intensity of the three broad lines individually. In the further analysis we will use the value centered on the recombination line, with the caution that this could under-predict the flux from the triplet as we held the FWHM frozen in the fit. Using the observed broad emission lines we can study the ionization distribution of the BLR. We do not detect highly ionized broad emission lines, evident from the lack of excess at the wavelengths around the Ne IX and Si XIII triplet, and Ne X and Si XIV Lyα lines.

6.3.2 UV broad emission lines

HST performed near simultaneous observations during this observing campaign, allowing to fit the UV and X-ray broad lines simultaneously. The UV broad emission lines in NGC 5548 are known to vary on timescales as short as a few days. As the *Chandra* campaign lasted for a week and we added all the X-ray data to detect the broad emission lines, this might cause complications in the analysis. In contrast the HST observations were shorter, and they are spread over 2 days, at the end of the X-ray

Table 6.1: Flux and the luminosity of the broad emission lines, from the simultaneous LETGS, Medium Energy Grating (MEG) and High Energy Grating (HEG) fit. The wavelength was frozen to the rest wavelength of the line, while the FWHM was frozen to 8000 km s^{-1}.

ion	λ (Å)	flux (ph m^{-2} s^{-1})	EW (mÅ)	log L W
C V f	41.421	1.0 ± 0.6	300 ± 180	34.2 ± 0.4
C V[a]	40.268	< 0.6	< 230	< 33.8
C VI	33.736	0.5 ± 0.2	150 ± 80	33.8 ± 0.2
N VII	24.781	< 0.05	< 70	< 32.9
O VII[b]	21.602	0.56 ± 0.13	130 ± 40	34.1 ± 0.1
O VIII	18.969	0.4 ± 0.2	60 ± 30	33.4 ± 0.3
O VII	18.627	0.19 ± 0.07	70 ± 30	33.5 ± 0.2

[a] This coincides with the instrumental C-edge, and could be due to possible calibration uncertainties.

[b] The resonance, intercombination and forbidden line significantly overlap and are fit as one blend.

observations.

We fit the UV broad lines using multiple Gaussians, leaving the normalization, the wavelength as well as the FWHM free parameters. We did not attempt a detailed profile fitting, rather we focused on obtaining reliable flux measurement for these lines so as to be able to model them with the photoionization codes. Table 6.2 lists the rest wavelength, the measured wavelength, flux and luminosity for the UV broad emission lines.

In the UV the O IV and Si III lines substantially overlap and thus we only list one flux value for this blend, although separate fluxes are given by Goad & Koratkar (1998). Also the 1218 Å O V, the 1215 Å He II, the 1221 Å Fe II and 1216 Å Fe XIII lines, and the 1216 Å Lyα line form a blend, and are reported as a blend. For the 1640 Å He II and 1892 Å Si III] lines we list an upper limit, as it is hard to deblend the narrow from the broad line component. For both lines the width of this line is smaller than the width of the other detected broad emission lines.

Table 6.2: The rest wavelength from Kelly (1987a, 1987b), with the exception of Mg II which was taken from CLOUDY, the measured wavelength, λ_{rest}, the fluxes and luminosities for the broad UV lines are listed. The errors in the listed luminosities are estimated to be 0.2 in log of the line luminosity, as systematic errors in continuum fit will dominate the errors in fluxes or luminosities.

ion	λ_{Kelly} Å	λ_{rest} Å	flux 10^{-15} W m^{-2}	log L W
Lyα, O V	1216, 1218	1222	2.8	35.6
He II, Fe II	1215, 1221	1222	2.8	35.6
Fe XIII	1216	1222	2.8	35.6
N V	1240	1239	0.5	34.8
Si IV, O IV]	1398, 1403	1398	0.3	34.5
N IV	1487	1485	0.1	33.9
C IV	1549	1547	3.8	35.7 5
He II[a]	1640	1639	0.09	33.8 5
O III	1666	1661	0.2	34.3
Si III][a]	1892	1891	0.02	33.3
C III]	1909	1903	0.6	34.9
Mg II	2798	2800	1.0	35.1

[a] This line is rather narrow and difficult to deblend from the narrow component. The measured line flux and luminosity is an upper limit.

6.4 Modeling the broad emission lines

We modeled the broad emission lines with two photoionization codes: XSTAR version 2.1h (Kallman & Krolik 1999) and CLOUDY version 95.06 (Ferland 2002).

In modeling the broad lines we used the same Spectral Energy Distribution (SED) (labeled Steenbrugge et al. in Fig. 6.2) as was used to study the warm absorber using the simultaneous HST-STIS spectra (Crenshaw et al. 2003) and *Chandra* spectra (Steenbrugge et al. 2004). As there is no evidence for a blue bump in the UV spectra, this bump was not included in our SED. For the X-ray part of the SED we used the continuum of the present LETGS spectrum. For the high energy part of the SED we used a power law component as measured in our *Chandra* spectrum but with an exponential cut-off at 130 keV, consistent with the previous Beppo*SAX* data (Nicastro et al. 2000). We did not include a reflection component in our SED, because the *Chandra* spectrum could not constrain it. Between 50 and 1000 Å we used a power-law and at even longer

wavelength we used the energy index of 2.5 adopted by Dumont et al. (1998).

For comparison we also plot in Fig. 6.2 the SED used by Goad & Koratkar (1998). The SED Goad & Koratkar (1998) has a lower high-energy cut-off of 65 keV (0.19 Å); and a higher low-energy cut-off of 1.2 eV(10^4 Å), thus producing less infrared radiation. The different results obtained for these different SEDs gives a good indication of how the ionization balance depends on the assumed SED, and will be discussed later.

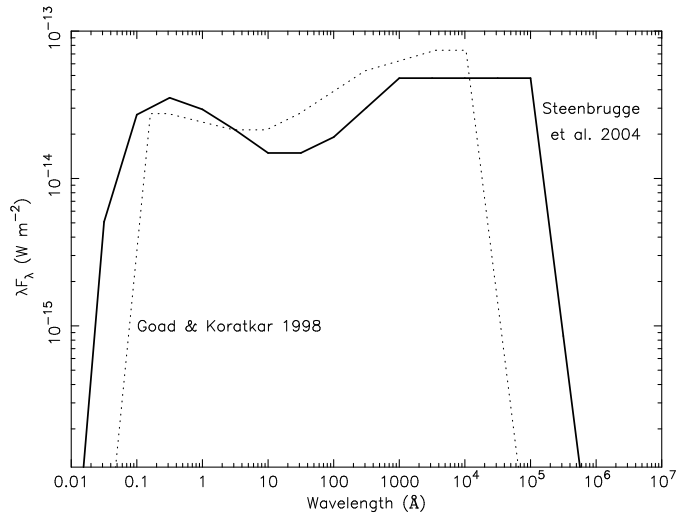

Figure 6.2: The SED used in the present analysis (solid line) and that used by Goad & Koratkar (1998) (dotted line).

As a starting point we took the ionization parameter, total hydrogen column density, density and temperature as deduced from the UV measurements of Goad & Koratkar (1998). We assumed their low state ionization parameter of $\log U = -0.6$ or $\log \xi = 1$ in units of 10^{-9} W m which will be used throughout the paper. In both codes we used the standard solar abundances as given in the CLOUDY code. In XSTAR only the following elements are included: H, He, C, N, O, Ne, Mg, Si, S, Ar, Ca, Fe and Ni, while CLOUDY lists all elements up to zinc. This difference is not expected to change the temperature structure of the gas and thus the ionization balance significantly. CLOUDY uses the values given in Grevesse & Sauval (2001) solar abundances, with the exception of C and O, for which it uses Allende Prieto et al. (2001, 2002), and N, Ne, Mg, Si and Fe, for which it uses Holweger (2001). In all models we assumed a

source luminosity of 1.91×10^{37} W (Goad & Koratkar 1998).

Goad & Koratkar (1998) list a broad Fe II feature at 2798 Å, but neither XSTAR nor CLOUDY list an Fe II line at 2798 Å. The measured luminosity should be used as an upper limit to the predicted value, if indeed there is an Fe II line at this wavelength. The Fe II and Fe XIII lines at 1216 Å are not included in XSTAR.

6.4.1 CLOUDY

As an initial trial we again used the parameters derived by Goad & Koratkar (1998) for the low luminosity state to model the broad lines. We will call this model the standard model, although this model shows large discrepancies with the data (see Fig. 6.3 and Table 6.3). Certainly for the X-ray lines, which are the lines with lower predicted luminosities, the match is poor. Most of the UV line luminosities are over-predicted; this is especially the case for N IV (1487 Å), Si III (1892 Å), He II (1640 Å) and O III (1666 Å). To investigate the sensitivity of these differences to the SED, we used the SED used by Goad & Koratkar (1998) instead of our own SED. The luminosities (triangles in Fig. 6.4 and model 3 in Table 6.3) are consistent with the results from the standard model within the measurement errors. Therefore the difference in SED can not explain the poor match.

Another difference may be the version of CLOUDY that is used. In model 2 (Table 6.3), we replace version 95.06 by the older 94 version (open diamonds in Fig. 6.4). The predictions of both versions of CLOUDY are shown in Fig. 6.3. This indeed gives some rather large differences, especially for the O VII triplet, the C V forbidden line and the Lyα blend. However, these differences can not explain the discrepancies obtained for some of the UV lines. Even if we use the UV fluxes as quoted by Goad & Koratkar (1998) we obtain poor agreement, although the agreement is better than with our present measurements.

A very important difference between the two versions of CLOUDY, is that the 94 version does not contain the O V line at 1218 Å. In the 95.06 version this line has a substantial flux, for the input parameters considered. The presence of this line, as well as possible S X, Fe XIII and Fe II can change the ionization parameter estimate for the broad line gas. Another difference occurs for the O VII triplet, where the 94 version had only two lines, with the total triplet luminosity three orders of magnitude weaker. This clearly indicates that the parameters as listed by Goad & Koratkar (1998) are probably not the best set to be used to model the X-ray and UV broad emission lines using the 95.06 version.

In order to be able to explain the measured line luminosities we need to understand how the predicted line luminosities change with varying parameters. Fig. 6.4 shows a comparison between our standard model (see Table 6.3 for a list of the input param-

Table 6.3: The measured luminosity (first column) versus the predicted luminosity for some of the different models described in the text. The standard model is indicated by the model name stan. CL stands for CLOUDY, XS for XSTAR. Our SED is shown as Steenbrugge et al. 2004, GK as Goad & Koratkar 1998 in Fig. 6.2. r is the distance of the cloud from the ionizing source, n the density of the gas, N_H the total column density, C_f is the covering factor.

	meas.	stan.	2	3	4	5	stan.	7	8	9
code		CL	CL	CL	CL	CL	XS	XS	XS	XS
vers.		95.06	94	95.06	95.06	95.06	2.1h	2.1h	2.1h	2.1h
SED		our	our	GK	our	our	our	GK	our	our
r (ld)		17	17	17	20	2	17	17	20	2
n^a		1	1	1	0.48	48	1	1	2.4	240
$N_H{}^b$		1	1	1	1	10	1	1	0.05	1
C_f		0.38	0.38	0.38	0.20	0.50	0.38	0.38	0.20	1.0
ξ		10	10	10	15	15	10	10	3	3
ion	log L (W)	log L (W)	log L (W)	log L (W)	log L (W)	log L (W)	log L (W)	log L (W)	log L (W)	log L (W)
C V f	34.2	33.9	31.5	33.6	33.8	32.4	34.9	34.9	34.5	34.6
C V	$<$ 33.8	33.1	31.5	33.2	32.9	33.2	33.7	33.7	33.9	34.5
C VI	33.8	33.2	33.3	33.4	33.1	33.5	34.3	34.2	33.8	34.2
N VII	$<$ 32.9	32.4	32.4	32.5	32.3	32.8	33.4	33.3	32.8	33.2
O VII t	34.1	34.8	31.9	34.9	34.7	35.1	35.0	35.0	34.3	34.6
O VIII	33.4	32.7	32.7	32.8	32.7	33.2	33.8	33.6	32.8	33.2
O VII	33.5	32.0	31.7	32.0	31.8	32.4	33.5	33.5	31.0	32.6
Lyα	35.6	35.0	34.4	35.1	35.7	35.5	36.2	36.2	35.6	35.6
N V	34.8	35.0	34.9	35.0	34.6	35.2	34.7	34.4	34.9	35.1
Si IV	34.5	35.1	35.1	35.0	34.6	35.1	35.6	35.5	34.7	35.3
N IV	33.9	34.7	34.6	34.6	34.4	34.2	34.5	34.5	33.8	33.4
C IV	35.7	35.9	35.9	35.9	35.6	35.5	35.8	35.8	35.7	35.4
He II	33.8	34.8	34.6	34.9	34.2	34.7	35.7	35.6	34.7	35.5
O III	34.4	35.2	35.2	35.1	34.8	34.5	34.4	34.3	33.4	33.8
Si III]	33.3	34.5	34.7	34.2	33.3	33.3	33.3	33.0	31 3	33.5
C III]	34.9	35.2	35.2	35.1	34.9	33.5	34.1	33.9	33.0	33.2
Mg II	35.1	34.2	34.2	34.2	33.4	33.5	34.4	34.3	31.0	34.5

^{a} in 10^{16} m^{-3}.
^{b} 10^{27} m^{-2}.

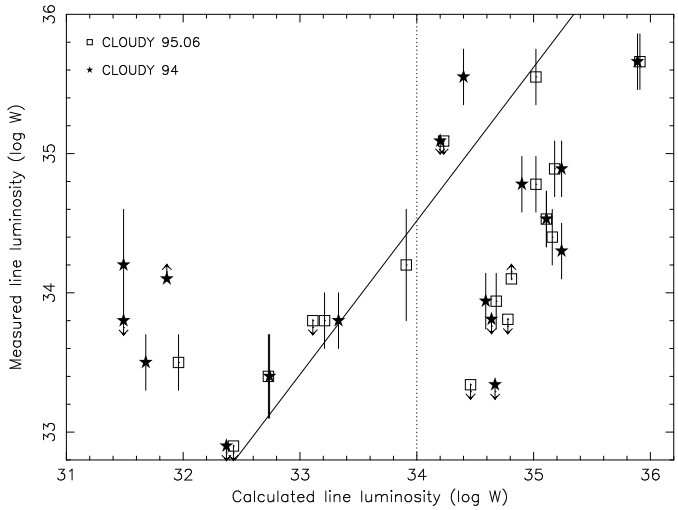

Figure 6.3: Comparison of the line luminosities calculated by CLOUDY versions 95.06 (open squares) and 94 (filled stars) and the measured line luminosity. All the lines for which CLOUDY 95.06 predicts less than 10^{34} W are X-ray lines. The lines to the right of the dotted line are UV lines with the exception of the O VII triplet. The solid line indicates a perfect match. Note that the match is rather poor for both versions of CLOUDY, even if the X-ray lines are ignored.

eters and predicted line luminosities) and other models tested. Note that the effect of covering factor (open squares), which we changed from 0.38 to 1, and the assumed SED (open triangles) are very minor on the calculated line luminosities. However, the covering factor does become important for lower covering factor values or higher ionization parameters. Also a model with lower density, but larger radius, such that the ionization parameter is the same (open circles), gives similar results as the standard model. This indicates that most line strengths are only weakly or not at all dependent on density. This is expected, as otherwise the density would be a known parameter. The spread in line luminosities for variations in ionization parameter are up to several orders of magnitude larger, the model with a lower ionization parameter (slanted crosses) or significantly higher ionization parameter (stars) give deviating line luminosities. A moderate increase in ionization parameter (crosses) is detectable in a few lines.

From Fig. 6.3 and Fig. 6.4 it is clear that a higher ionization parameter is needed to fit the measured luminosities. Namely, the luminosities measured in the X-rays are

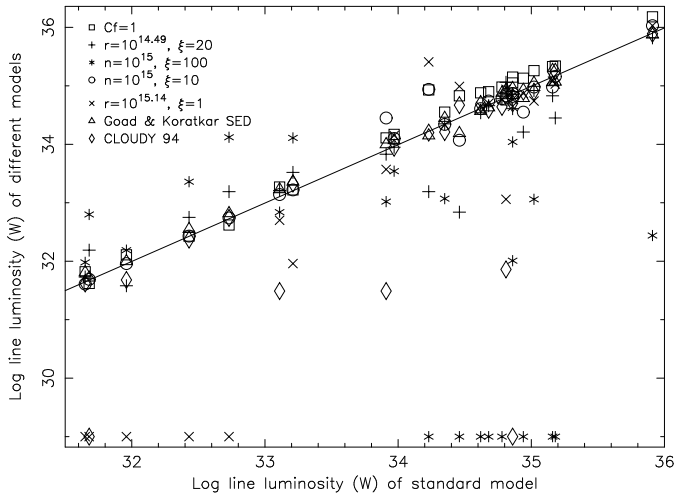

Figure 6.4: A comparison of the line luminosities as calculated by the standard model (see Table 6.3) and other models. Open squares denote a covering factor of 1, crosses for a radius of 12 ld, resulting in a higher ionization parameter of ξ = 20. Asterisks denote a lower density, namely 10^{15} m^{-3}, resulting in an ionization parameter of ξ = 100. Open circles denote a 10^{15} m^{-3} density, but with a radius of 53 ld and thus ξ = 10. The slanted crosses are for a radius of 53 ld, with a density of 10^{16} m^{-3} and thus ξ = 1. Finally the triangles depict the SED assumed by Goad & Koratkar (1998) and the diamonds are for the standard input parameters, but for CLOUDY version 94. A value of log L = 10^{29} W indicates that this value was not calculated by CLOUDY in this particular run. The solid line indicates where the line luminosity are equal for both models.

underpredicted, while those in the UV are overpredicted. To have a physical basis, we made models for a distance of 2 light days (ld), the shortest distance listed from reverberation mapping of He II (Peterson & Wandel 1999); and 20 light days, the distance obtained from reverberation mapping of Hβ (Peterson et al. 1994). For both assumptions we can model the measured broad emission lines with one ionization parameter, ξ = 15. The resulting match for both distances is plotted in Fig. 6.5.

In the case of a distance of 20 ld, we can model the observed line luminosities rather well with one ionization parameters (open squares in Fig. 6.5). There is actually a range in density (and thus ionization parameter) for which we obtain a reasonable

match. In the case of a distance of 2 ld (open stars in Fig. 6.5), the match is worse. If only one ionization parameter is assumed, there are always several ions poorly fit. This worsening in fit is solely dependent on the large density necessary for such a short distance. For the 2 ld match we need to increase the total hydrogen column density by a factor of 10 and the covering factor by a factor of 2.5, as otherwise the line luminosities are systematically underpredicted. This underprediction holds for all the lines, and cannot be improved by a change in ionization parameter. A line luminosity that is overpredicted in all models is the He II line at 1640 Å, which is the only line that is variable on timescales as short as 2 ld (Peterson & Wandel 1999). The O VII triplet is also consistently overpredicted, but this seems the result of not implementing all triplet processes in the CLOUDY code. As we will see later, XSTAR finds a better match. If we assume the SED used by Goad & Koratkar (1998), we find a very similar match, thus confirming that a different SED only changes the predicted line luminosities slightly.

It thus would seem that one needs at least 2 different ionization parameters to model the line luminosities, if one assumes the lines are formed at a distance of only 2 ld. However, from reverberation mapping we know that most lines are formed further out. Thus the density is substantially smaller, and the line luminosities are less dependent on density effects. Assuming a two ionization model, we have the problem that one ionization parameter already produces too much He II. He II is one of the ions that is formed over a large range in ionization parameter. To reduce the He II line luminosity, we would need to have a substantially higher ionization parameter. However, the limit to the ionization parameter is set by the lack of highly ionized X-ray lines. Both conditions make a two ionization parameter model less likely. A possible explanation for the overprediction in He II line luminosity is that the line is more readily destroyed than currently assumed. An interesting difference between the models for 20 ld and 2 ld is that, due to the larger covering factor and higher density in the 2 ld model, a part of the 1216 Å broad emission line should be due to Fe II. This line is not included in the 20 ld model.

6.4.2 XSTAR

We followed a similar approach in modeling the broad emission lines using XSTAR as for CLOUDY. First we used the input parameters listed by Goad & Koratkar (1998) but with our SED, called the standard model (Table 6.3). In Fig. 6.6 we plot the calculated and measured line luminosity. The match is similarly poor to that obtained with CLOUDY. The match to the UV data is not as good as with CLOUDY; however, the match to the X-ray data is significantly better than with CLOUDY. In general XSTAR overpredicts the UV line luminosities, but from Fig. 6.6 a one ionization parameter

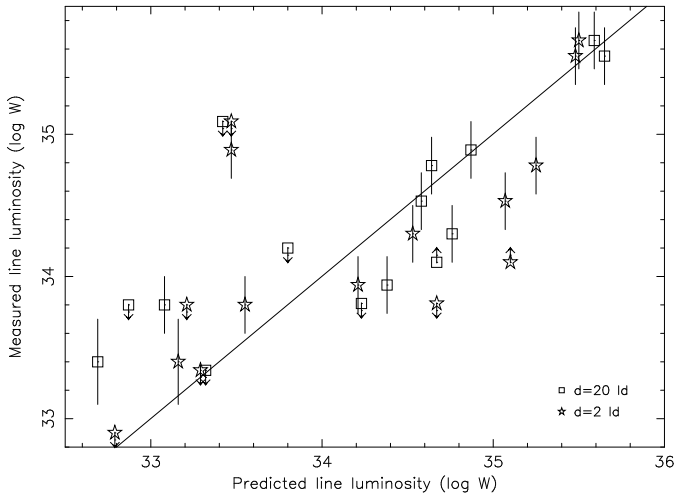

Figure 6.5: Results for our best match between line luminosities predicted by the CLOUDY code and the measured line luminosities. The open squares are for a cloud at a distance of 20 ld, the open stars are for a distance of 2 ld. The parameters are listed in Table 6.3, model 4 and 5. The O VII triplet is indicated as a lower limit (see text), the Mg II line, probably a blend is indicated as a upper limit. The other upper limits are measured upper limits.

model seems plausible.

For XSTAR we also compared our standard model with other models which have one parameter altered (see Fig. 6.7). The difference in abundances used (open stars), the SED used (open triangles) or a lower density (open circles) do not alter the predicted line luminosities. The difference in covering fraction (open squares) is larger than in the study with CLOUDY, albeit still rather small. Similar to the results obtained with CLOUDY the difference in ionization parameter (crosses, slanted crosses and asterisks) give the largest differences in line luminosities. In general the differences in predicted line luminosity with XSTAR are similarly dependent on the input parameters, as with CLOUDY.

We generated models for cloud distances of 20 ld and 2 ld with XSTAR. To start, we took the parameters for our best match obtained with CLOUDY for a distance of 20 ld. The XSTAR-predicted line luminosities in this case give a rather poor match to the measured line luminosities. Most noticeable are the discrepancies for the 1640 Å He II

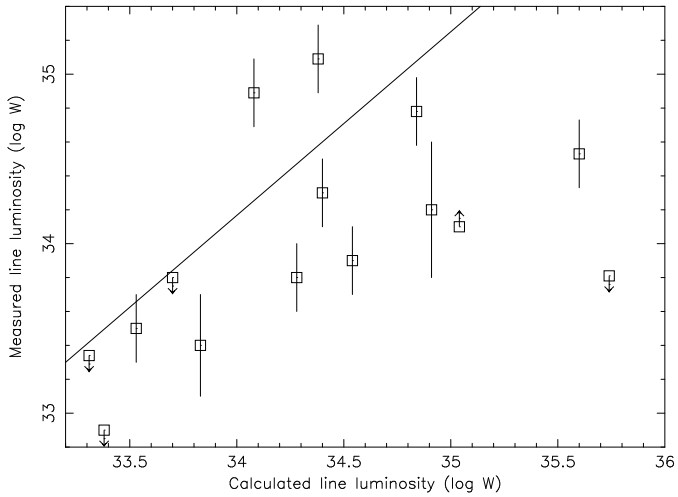

Figure 6.6: The XSTAR calculated line luminosities for the standard model versus the measured line luminosities. Note that the match for the predicted weaker lines, mostly X-ray lines, is decent, but that the match for the lines predicted to have larger luminosities is poor.

line, the 1487 N IV line, the O VII triplet, the 1216 Å blend and the blend due to Si IV and O IV at about 1400 Å. This is in line with the difference in predicted luminosities for the standard model (see Fig. 6.8). In general, from Fig. 6.6 we find that an ionization parameter similar to the value in the standard model or lower is required.

For a distance of 20 ld, our best model (Table 6.3 model 8 and Fig. 6.9) predicts indeed a rather low ionization parameter of $\xi = 3$ ($\log \xi = 0.477$), with a lower total column density. A change in ionization parameter at such a low ionization parameter, is very noticeable. Even small changes in column density are noticeable, and as a result we do not have a range of possible values for a good match, unlike the results obtained with CLOUDY. Although the column density, the ionization parameter and thus the density are different from the values obtained with CLOUDY, the covering factor is similar. A large difference between XSTAR and CLOUDY is the predicted line luminosities for the C III line at 1909 Å and the O III line at 1666 Å, which are both severely underpredicted by XSTAR. Similar to the results obtained with CLOUDY, the He II line at 1640 Å is overpredicted. We need a higher ionization parameter and a lower total column density to obtain a good match for He II. However, in such models

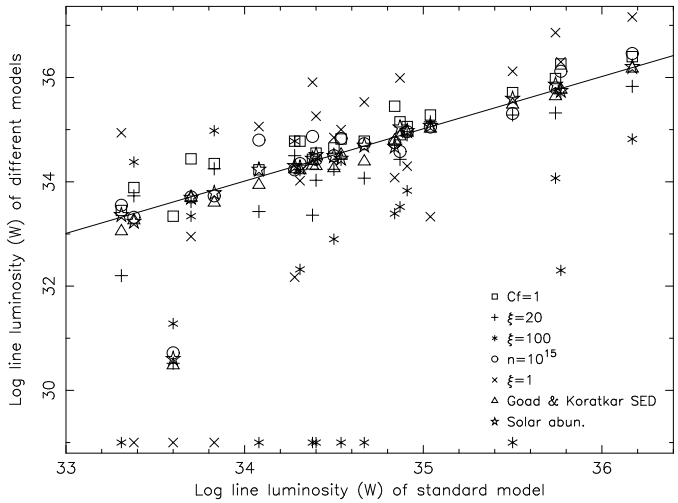

Figure 6.7: Comparison of the line luminosities predicted by the standard model and models with one parameter altered. In this plot O VIII is missing, due to the low predicted luminosity for the standard model. Symbols are the same as in Fig. 6.5. Open squares is for a covering faction of 1, crosses are for a ξ value of 20, asterisks for ξ = 100. Open circles are for a density of 10^{15} m^{-3}, slanted crosses for ξ = 1. Open triangles are for the SED assumed by Goad & Koratkar (1998) and open stars are for the standard solar abundances assumed by XSTAR.

the 1216 Å blend is severely underpredicted, and other broad emission lines, such as O VIII are overpredicted. Similar to our CLOUDY results, a two ionization model seems unlikely due to the limit of the highest ionization parameter possible, and the fact that He II is produced over a larger ionization range.

For the best model assuming a distance of 2 ld (Table 6.3 model 9 and Fig. 6.9), the covering factor needs to be increased. Consistent with our results from CLOUDY, a density increase of 100 does noticeably change the predicted line luminosities, and the best match covering factor and total column density are thus different for the two distances. If the column density and covering factor were not increased, the line strengths are systematically underpredicted. Also consistent with our CLOUDY result is the fact that the 2 ld model gives a poorer match to the measured line luminosities than the 20 ld model.

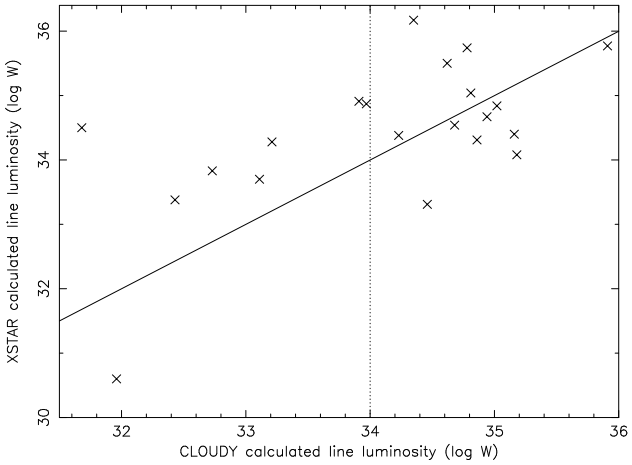

Figure 6.8: A comparison of the predicted line luminosities using our standard model (Table 6.3) for CLOUDY and XSTAR. The solid line indicates equal line strengths. The dotted line indicates the distinction between X-ray (with lower predicted CLOUDY luminosity) and the UV lines and the O VII triplet. Note the systematic difference between both codes for the X-ray lines, and a scatter for the UV lines.

6.5 Discussion

Comparison between CLOUDY and XSTAR

Comparing the predicted line luminosities obtained with CLOUDY and XSTAR for the standard model (see Fig. 6.8, Table 6.3), we find that XSTAR systematically predicts higher luminosities for the X-ray lines, with the exception of O VIII Lyα. The XSTAR values for the UV lines cluster around the CLOUDY values, which are larger than for the X-ra lines. However, the predicted line luminosities for individual UV lines can significantly differ between both codes. Clearly, the differences in the luminosities obtained with CLOUDY and XSTAR are larger than differences produced by possible changes in covering factor or assumed SED. This is also the conclusion we draw from comparing the difference in ionization parameter and column density obtained with both codes.

An important difference between both codes is the 1218 Å O V, the 1216 Å Fe XIII and 1221 Å Fe II lines. Not including these lines will affect the model ionization parameter obtained from the 1216 Å blend, which mostly consists of H I Lyα. This might

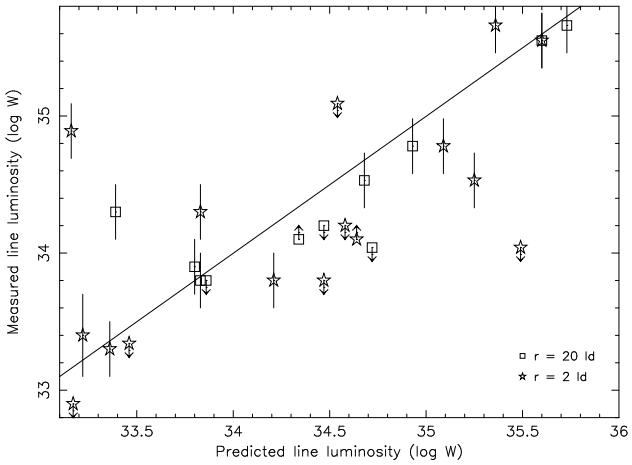

Figure 6.9: The best fit obtained with the XSTAR code for a distance of 20 ld (open squares) and 2 ld (open stars), for which the parameters are listed in Table 6.3 model 8 and 9. The line luminosity predictions for Si III, the O VII line at 18.63 Å and the Mg II 2798 Å line fall for the 20 ld model below $10^{32.5}$ W. Note that the differences between in line luminosities for the different distances are very similar to the differences obtained with CLOUDY (Fig. 6.5).

be the reason why XSTAR gives a lower ionization parameter. Interestingly, we find a good match to the 1216 Å blend with both codes for both distances. It is for the unblended C III and O III lines that we find a poor match with XSTAR.

To further investigate these differences, we compared how the predicted line luminosities change between the different distance models in both codes. For both codes we find an increase in covering factor, a higher column density and the same ionization parameter for the lower distance model. The differences in predicted line luminosities for the different distance models mimic each other as well (see Fig. 6.5 and Fig. 6.9). So does the predicted luminosity increase in the lower distance model for the O VII triplet, the O VII line at 18.63 Å, He II, N V, the Si IV and O IV blend, O VIII Lyα line, Si III, Mg II, C VI and N VII. There is a decrease in predicted luminosity for the C V forbidden line. The only difference between the codes is for C III, which increases in XSTAR, while decreasing in CLOUDY. However, note that this line is not well predicted with XSTAR. The correlation in line strengths with density gives confidence that, although we obtain different parameters from the different codes, the basic physics applied is

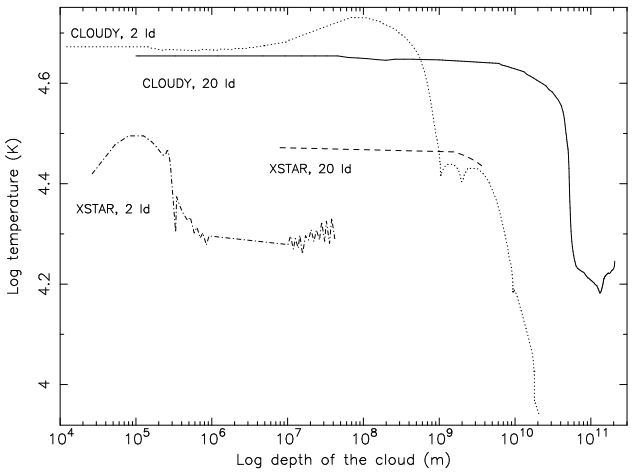

Figure 6.10: The temperature as a function of the depth of the cloud for a distance of 20 ld (solid line for CLOUDY prediction, dashed line for XSTAR prediction) and 2 ld (dotted line for CLOUDY prediction, dash-dotted line for XSTAR prediction). Note the broad dip between 5×10^{10} m and 2×10^{11} m in the 20 ld CLOUDY model that corresponds with the peak in fractional abundance for C IV (see Fig. 6.11). There is a smaller dip between 10^9 m and 2×10^9 m in the 2 ld CLOUDY model corresponding to the C IV peak in fractional abundances (see Fig. 6.12).

similar and the difference is a calibration problem between the codes.

Both codes have a problem with predicting the line luminosity for He II, and in both cases the match worsens for the 2 ld model. As we have already discussed, the UV and X-ray broad emission lines can be modeled with one ionization parameter and density, and thus one expects that all these lines are emitted from the same distance. However, the reverberation distances for the UV ions are not the same. From our modeling of the broad emission lines we find that He II is formed over a large range of ionization parameters, but is most efficiently formed at very low ionization parameter. It is thus counter-intuitive that He II does has the shortest reverberation mapping distance. This problem needs further investigation.

The fact that we need a higher total column density and covering factor for the 2 ld models, is consistent with a picture where our line of sight crosses the edge of a rotating cloud.

Temperature of the absorbing cloud

We can study the temperature (see Fig. 6.10) and the fractional ion abundance (see Fig. 6.11 to Fig. 6.14) as a function of depth of the cloud for both distance models. Comparing both codes we find that the cloud depth for our results is about two orders of magnitude smaller in XSTAR. Due to the higher density, the depth of the cloud for the 2 ld distance model is smaller in both codes. From the calculations by CLOUDY we see that the cloud for the 2 ld distance model is hotter near the illuminated side, but shows a rather steep drop at $\sim 7 \times 10^8$ m. The cloud at 20 ld has a less drastic drop in temperature further into the cloud, and seems to recover at the non-illuminated side of the cloud. With XSTAR we find a significantly lower temperature for both distance models. The temperature of the 2 ld model has a similar increase in temperature near the illuminated surface, and a decrease in temperature at a similar cloud depth as has the CLOUDY model for the same distance. However, in XSTAR the temperature levels off for this distance, while the temperature for the CLOUDY model still decreases.

Fractional abundances

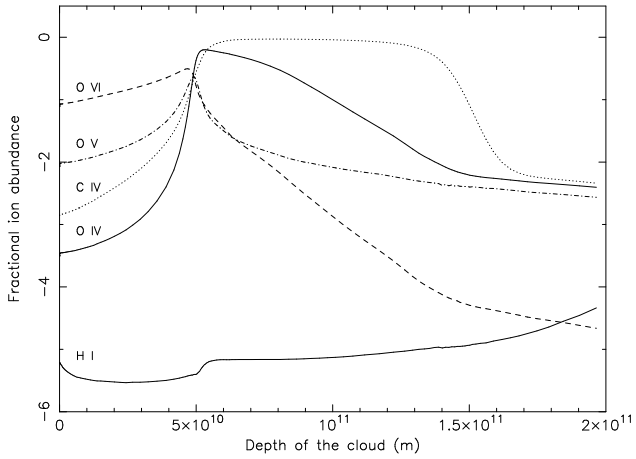

Figure 6.11: The fractional abundances (given as logs) versus the depth of the cloud for O IV, H I (solid lines), C IV (dotted line), O VI (dashed line), and O V (dash-dotted line) for the 20 ld model. Note the range in depth of the cloud for which C IV has a high fractional abundance. This broad peak corresponds to a broad dip in temperature (see Fig. 6.10).

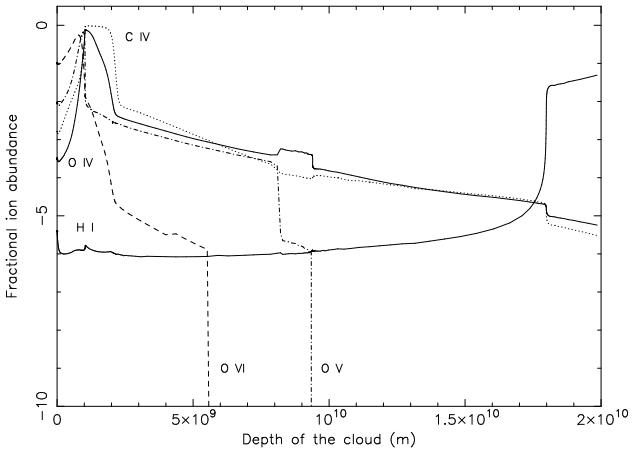

Figure 6.12: Same as Fig. 6.11, but for the 2 ld model. Note the smaller depth of the cloud and the strong increase of H I at the unilluminated edge of the cloud.

Both codes calculate fractional abundances as a function of depth in the cloud. The fractional abundances of H I, C IV, O IV, O V and O VI for both distance models and both codes are plotted in Fig. 6.11 to Fig. 6.14. For a distance of 20 ld CLOUDY finds a peak in fractional ion abundance at about 5×10^{10} m, with the exception of H I which peaks near the non illuminated edge of the cloud. C IV has a high fractional ion abundance over a large part of the cloud, which explains why this is the most luminous line detected in the UV and X-ray band. For the 2 ld distance model the fractional ion abundances peak much closer to the illuminated edge of the cloud. Again H I peaks at the non illuminated face of the cloud, but the cloud is much smaller. The profiles of the fractional ion abundance curves are similar, but in absolute scale much smaller than for the 20 ld distance model. H I has a much stronger peak at the non illuminated edge of the cloud, which compensates for the lack of Fe XIII and S X in the 1216 Å blend.

Using the best match parameters we find different fractional abundances as a function of depth in the cloud with XSTAR than with CLOUDY. The fractional ion abundances obtained with XSTAR are about an order of magnitude larger at the illuminated face of the cloud, with the exception of H I. In the 20 ld model, due to the low total column density, we find a slight increase in fractional abundances for all ions except H I. The results for the 2 ld model are more similar to the results obtained with CLOUDY. This similarity is due to the larger total column density used in this model. Thus the physical parameters in the cloud are different for XSTAR and CLOUDY.

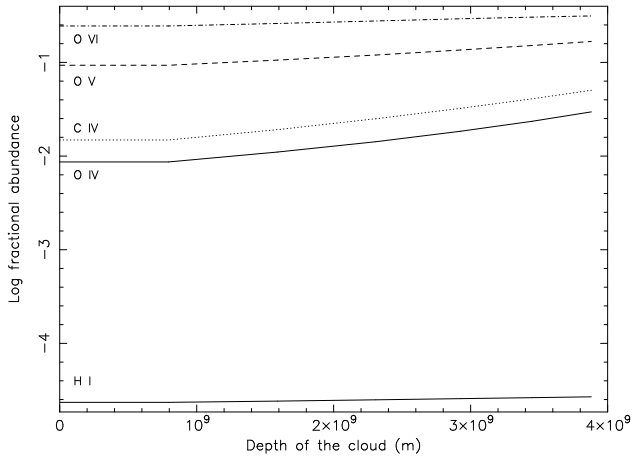

Figure 6.13: Same as Fig. 6.11, but now calculated by XSTAR. Note the very different result compared to the CLOUDY result for a 20 ld distance.

Comparison with other X-ray observations

Comparing our results with the earlier results on NGC 5548 (Kaastra et al. 2002a) we find a much weaker line in our data, with a similar FWHM. Kaastra et al. (2002a) detected a broad C VI Lyα emission line, with a derived flux of $5.6^{+3.5}_{-1.7}$ photons m^{-2} s^{-1}, an order of magnitude larger than the flux measured from the 2002 LETGS spectrum which is 0.5 ± 0.2. The FWHM of 10600 km s^{-1} $\pm$ 3300 km s^{-1} is consistent with the FWHM we assumed. In NGC 4051 Ogle et al (2004) find a broad O VII resonance line and a C VI Lyα emission line with a FWHM of 11000 km s^{-1} $\pm$ 3000 km s^{-1} and 1200 km s^{-1} $\pm$ 70 km s^{-1} respectively. The width of the C VI line is much narrower than the lines we detect, however, the width for the O VII resonance line is very similar to our assumed 8000 km s^{-1}.

6.6 Summary

We determined how the line luminosity calculated by the photoionization codes CLOUDY and XSTAR is dependent on the density, abundances, covering factor, ionization parameter, total column density and SED assumed. The line luminosity is nearly independent of abundances and the SED for the parameters tested. The line

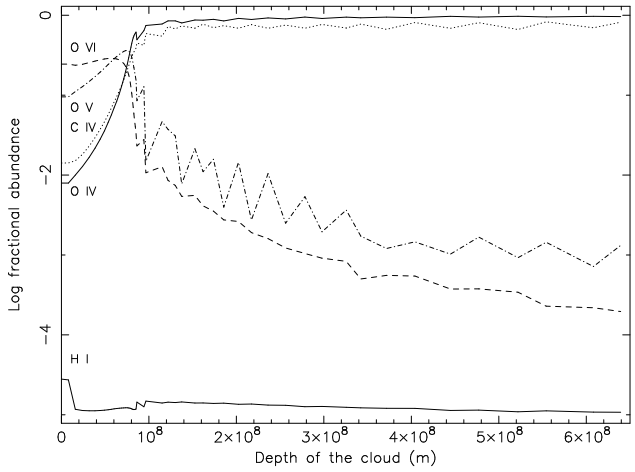

Figure 6.14: Same as Fig. 6.11, but for the 2 ld model and calculated by XSTAR.

luminosity is dependent on the covering factor if less than 5 %; and the density and column density, if the density is more than 10^{18} m^{-3}. We modeled the lines for a cloud distance of 20 ld and 2 ld. We can model the broad emission lines detected in the simultaneous *Chandra* and HST STIS observations with one ionization parameter. However, this ionization parameter differs from ξ = 15 for CLOUDY to ξ = 3 for XSTAR. The temperature, ion abundance profiles and the size of the cloud are different in both codes. In both codes the match in the 20 ld model is better, has a lower total column density and covering factor. This is consistent with a flattened rotating structure which we observe through the edge.

Acknowledgments SRON National Institute for Space Research is supported financially by NWO, the Netherlands Organization for Scientific Research.

References

Allende Prieto, C., Lambert, D. L. & Asplund, M., 2001, ApJ, 556, L63

Allende Prietro, C., Lambert, D. L. & Asplund, M., 2001, ApJ, 573, L137

Anders, E. & Grevesse, N., 1989, Geochim. Cosmochim. Acta, 53, 197

Arav, N., Barlow, T. A., Laor, A., et al., 1998, MNRAS, 297, 990

Arav, N., Korista, K. T. & de Kool, M., 2002, ApJ, 566, 699
Arav, N., Gabel, J., Kaastra, J. S., et al., 2004, in preparation
Blandford, R. D. & McKee, C. F., 1982, ApJ, 255, 419
Branduardi-Raymont, G., Sako, M., Kahn, S. M., et al., 2001, A&A, 365, 140
Costantini, E., Kaastra, J. S., Steenbrugge, K. C., et al., in prep.
Crenshaw, D. M. & Kraemer, S. B., 1999, ApJ, 521, 572
Crenshaw, D. M., Kraemer, S. B., Gabel, J. R., et al., 2003, 594, 116
Dumont, A-M., Collin-Souffrin, S. & Nazarova, L., 1998, A&A, 331, 11
Elvis, M., 2000, ApJ, 545, 63
Ferland, G. J., 2002, *Hazy, A Brief Introduction to Cloudy 96*, http://www.pa.uky.edu/∼gary/cloudy
Goad, M. & Koratkar, A., 1998, ApJ, 495, 718
Grevesse, N. & Sauval, A. J., 2001, Space Science Review, 85, 161
Hewitt, A., Burbidge, G., 1991, ApJS, 75, 297
Holweger, H., 2001, Joint SOHO/ACE workshop: "solar and Galactic Composition".
Kaastra, J. S. & Barr, P., 1989, A&A, 226, 59
Kaastra, J. S., Steenbrugge, K. C., Raassen, A. J. J., et al., 2002a, A&A, 386, 427
Kaastra, J. S., Mewe, R. & Raassen, A. J. J., 2002b, Proceedings Symposium 'New Visions of the X-ray Universe in the XMM-*Newton* and *Chandra* Era'
Kaastra, J. S., Arav, N., Steenbrugge, K. C., 2004, in preparation
Kallman, T. R. & Krolik, J. H., 1999, XSTAR photoionization code, ftp://legacy.gsfc.nasa.gov/software/plasma_codes/xstar/
Kelly, R. L., 1987, Journal of Physical and Chemical Reference Data, Vol. 16 Suppl. 1
Kelly, R. L., 1987, Journal of Physical and Chemical Reference Data, Vol. 16 Suppl. 2
McKee, C. F. & Tarter, C. B., 1975, 202, 306
Nandra, K., Fabian, A. C., George, I. M., et al., 1993, MNRAS, 260, 504
Nicastro, F., Piro, L., De Rosa, A., et al., 2000, ApJ, 536, 718
Ogle, P. M., Mason, K. O., Page, M. J., et al., 2004, ApJ, 606, 151
Peterson, B. M., 1994, ASP Conference Series, Vol. 69
Peterson, B. M. & Wandel, A., 1999, ApJ, 521, L95
Seyfert, C. K., 1943, ApJ, 97, 28
Steenbrugge, K. C., Kaastra, J. S., de Vries, C. P. & Edelson, R., 2003, A&A, 402, 477
Steenbrugge, K. C., Kaastra, J. S., Crenshaw, D. M., submitted to A&A
Tanaka, Y., Nandra, K., Fabian, A. C., et al., 1995, Nature, 375, 659
Wilms, J., Reynolds, C. S., Begelman, M. C., et al. 2001, MNRAS, 328, 27